RESEARCH ARTICLE

Redox gradients at the low oxygen boundary of lakes

Mathias K. Kirf · Hans Røy · Moritz Holtappels · Jan P. Fischer · Carsten J. Schubert · Bernhard Wehrli

Abstract The distribution of oxygen (O_2) at the oxic/anoxic interface in the water column of two Swiss lakes was measured with sub-micromolar sensitivity, high precision, and high spatial resolution. The O_2 distribution was found to be highly variable and it is shown that N-cycling and the redox gradients of Mn, Fe and CH_4 are controlled by O_2 distributions down to the nanomolar concentration range. The profiles reveal that apparent gaps between the oxic zone and the sites of CH_4 and Mn oxidation are bridged by zones with $0.01-1$ μmol L^{-1} O_2 concentrations and thus CH_4 and Mn oxidation clearly occur at oxic conditions. Directly below the steep oxycline of Lake Rot a broad low O_2 zone in the depth range of $6-7.5$ m was now detectable. The O_2 increase during daylight in this zone was comparable to the O_2 flux along the oxycline. Here photosynthesis could be responsible for a substantial part of the chemotrophic oxidation processes. An even broader zone ($0.8-3.8$ m) with sub-micromolar O_2 and evidence for methanotrophic and lithotrophic activities found at 160 m depth in the deep, dark hypolimnion of Lake Zug was maintained by transport, reaction- and mixing processes. The submicromolar zones could not have been resolved with traditional CTD-profiles. Their existence expands the oxic zone downwards and implies that substantial parts of "suboxic zones" characterized by the absence of both O_2 and H_2S may actually belong to the realm of oxic processes if more sensitive measurement techniques are used for their characterization.

M. K. Kirf (✉) · C. J. Schubert · B. Wehrli
Department of Surface Waters, Research and Management,
Eawag, Swiss Federal Institute of Aquatic Science and
Technology, Seestrasse 79, 6047 Kastanienbaum, Switzerland
e-mail: mathias@kirf.de

M. K. Kirf · B. Wehrli
Institute of Biogeochemistry and Pollutant Dynamics, ETH
Zurich, Universitätsstrasse 16, 8092 Zurich, Switzerland

H. Røy
Center for Geomicrobiology, Department of Bioscience, Aarhus
University, Ny Munkegade 116, 8000 Aarhus C, Denmark
e-mail: hans.roy@biology.au.dk

M. Holtappels
Department of Biogeochemistry, Max Planck Institute for
Marine Microbiology, Celsiusstrasse 1, 28359 Bremen, Germany
e-mail: mholtapp@mpi-bremen.de

J. P. Fischer
Institute of Analytical Chemistry and Food Chemistry, Graz
University of Technology, Stremayrgasse 9, 8010 Graz, Austria
e-mail: fischer@tugraz.at

Introduction

Most aquatic animals cannot sustain oxic respiration below ~ 60 μmol O_2 L^{-1} (Gray et al. 2002; Keeling et al. 2010) and this limit can be used to define hypoxia in aquatic environments. Only below ~ 5 μmol O_2 L^{-1}, however, does NO_3^- become a preferred terminal electron acceptor (TEA) for facultative aerobic microorganisms, and aerobic microbial respiration continues without kinetic limitation down to the nanomolar range (Stolper et al. 2010). Thus, there is ample space for complex redox cycling at or below

the detection limit of traditional analytical techniques at around 1 μmol L^{-1} (Berner 1981; Canfield and Thamdrup 2009). Indeed, marine in situ studies with Switchable Trace O$_2$ (STOX)—sensors (Revsbech et al. 2009; Kalvelage et al. 2011; Thamdrup et al. 2012) indicated that a detection limit of 1 μmol O$_2$ L^{-1} is by at least one order of magnitude too high to adequately detect and classify O$_2$ dependent redox-interactions in natural systems.

Redox cycling at very low O$_2$ concentrations is relevant for oxic/anoxic interfaces in sediments and water columns. Both, the production and the removal of major greenhouse-gases (CH$_4$, N$_2$O; Lashof and Ahuja 1990) as well as the loss of reactive nitrogen from biological systems are strongly related to such O$_2$-induced changes in the TEA (Seitzinger et al. 1984; Mulder et al. 1995; Lam and Kuypers 2011). A multitude of transformation pathways can co-occur at oxic/anoxic interfaces interconnecting the cycles of different elements (Lam and Kuypers 2011; Kalvelage et al. 2011).

In this study, the oxic/anoxic transition in two Swiss lakes, holomictic Lake Rot and meromictic Lake Zug is explored in detail using a custom made profiling in-situ analyzer (PIA) (Kirf et al. 2013). The PIA enables continuous high-resolution profiling across steep oxic/anoxic transitions with sensitivity in the nanomolar range and online data-monitoring to allow targeted sampling. Snapshots of chemical gradients are presented together with submicromolar O$_2$ profiles in order to investigate how submicromolar O$_2$ concentrations interact with the cycling of N, Mn, Fe, S and CH$_4$ and whether the applied sensors can resolve the relevant range of O$_2$ concentrations. The high-resolution O$_2$ profiles revealed previously unnoticed, extensive and highly variably zones of submicromolar O$_2$ concentrations, where important redox transformations, e.g. CH$_4$-oxidation or nitrification, can occur.

Materials and methods

Study sites

Studies were conducted in two Swiss lakes chosen for their different stratification. Lake Rot is seasonally stratified with a steep thermocline that co-occurs with the oxic/anoxic interface. In Lake Zug, the oxic/anoxic transition occurs deep in the permanently, but weakly stratified hypolimnion.

Lake Rot (47.07°N, 8.32°E) is a holomictic eutrophic prealpine lake close to the city of Lucerne, Switzerland with a surface area of 0.46 km^2, a volume of 0.0039 km^3 and a mean hydraulic residence time of 0.4 year (Kohler et al. 1984). Measurements were performed in the deepest part of the lake (~16 m, online resource 1). The lake is shielded from winds and a stable stratification (gradient of
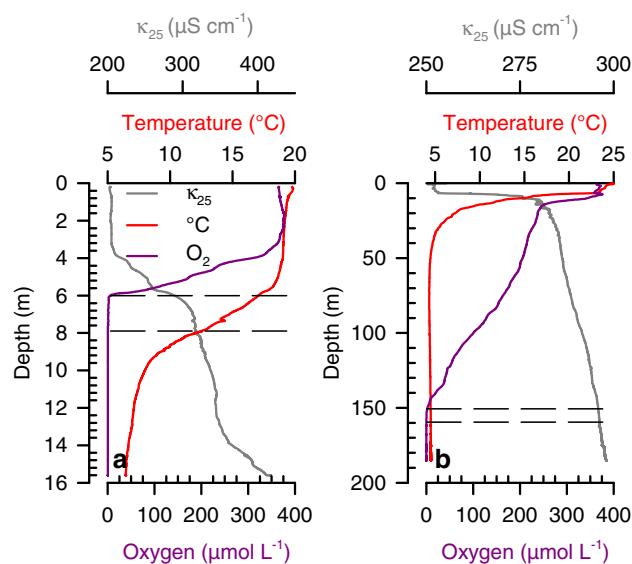
Fig. 1 Synoptical profiles of the physical gradients and the O$_2$-distribution in the water column of Lake Rot (**a**) and Lake Zug (**b**). *Dashed lines* indicate zones with low to submicromolar O$_2$ concentrations

temperature (ΔT) ~ –2 °C m^{-1}, gradient of specific conductivity (corrected to 25 °C, Δk_{25}) ~10 μS cm^{-1} m^{-1}) establishes between May and November with a strong chemocline at 8–11 m and an euxinic hypolimnion (Schubert et al. 2010) (Fig. 1a).

Meromictic Lake Zug (47.10°N, 8.48°E) in central Switzerland has a maximum depth of 198 m, a surface area of 38.3 km^2, a volume of 3.2 km^3 and a mean hydraulic residence time of ~14 years (Maerki et al. 2009). Measurements have been performed near the deepest site (198 m) in the south basin (online resource 1) which is shielded from westerly winds by high mountains and not influenced by the main inflow. Lake Zug remains permanently anoxic below 160 m despite a weakly stratified hypolimnion with a weak, reversed temperature gradient below 80 m ($\Delta T < 0.002$ °C m^{-1}, $\Delta k_{25} < 0.1$ μS cm^{-1} m^{-1}) (Fig. 1b) caused by the geothermal heat flux.

Profiling in-situ analyzer (PIA)

All in situ measurements and the online-controlled water sampling was performed with the PIA (Kirf et al. 2013). It is equipped with two independent O$_2$ sensor systems optimized for low O$_2$ concentrations based on microoptodes (TOS7-dye, 140 μm tip-diameter, white optical isolation, PreSens) and clark-type amperometric O$_2$ microsensors (Ox-25, Unisense). In this study, the optical sensors with a response time of 7 s were used to resolve submicromolar O$_2$ concentrations.

Instruments were mounted at the outside of an open cubic aluminium-frame of 50 × 50 × 60 cm which held

on its top the central processing unit and its power supply and left room in the centre for a carousel syringe sampler (KC Denmark) with 12×60 ml plastic syringes (Omnifix, B. Brown). If a higher sampling-volume was preferred over a higher number of samplings per cast, a custom-made actuator allowed simultaneous sampling of multiple syringes at a given depth. Two-way communication along a galvanically isolated load-carrying data-cable allowed online evaluation of depth-profiles on shipboard via a laptop computer and enabled targeted sampling. Using an electrical winch, profiles were recorded with dive speeds between 0.2 and 0.9 m min^{-1} in Lake Rot and between 1.0 and 3.6 m min^{-1} in Lake Zug (see online resource 2). Between profiles, the boat-position was changed by several meters to an undisturbed spot.

O$_2$ measurements

Pressure, conductivity and temperature were recorded by a CTD (XR-420, RBR) with a sampling rate of 2 Hz. The microoptode was calibrated to O$_2$ partial pressure based on the Stern–Volmer equation (Lippitsch et al. 1988) by a two point calibration in the laboratory with nanopure water (4 °C) equilibrated with certified gas mixtures (0.00 and 1.59 % O$_2$; PanGas) for the anoxic and the oxic calibration point, respectively. The obtained curve was recalibrated in situ with a one point calibration at anoxic in situ conditions. The microoptodes were sampled at 1 Hz and the in situ detection limits (calculated as two times the standard deviation in the anoxic water column) were 12.4 ± 0.5 nmol O$_2$ L^{-1} ($n = 9$) for the microoptode used on 6 August 2010 in Lake Zug and 8.4 ± 0.6 nmol O$_2$ L^{-1} ($n = 13$) and 8.3 ± 0.8 nmol O$_2$ L^{-1} ($n = 9$) for the microoptode used on 25 August 2010 in Lake Zug and on 14 September 2010 in Lake Rot, respectively. O$_2$ concentrations above 35 µmol L^{-1} were measured with amperometric microsensors, which were calibrated by a linear two-point in situ calibration using Winkler-derived (Winkler 1888) epilimnetic O$_2$-concentrations and the anoxic water column (Kirf et al. 2013).

The O$_2$ partial pressure in water was related to O$_2$ concentrations $C_{O_2}^*$ at standard pressure p* of 101,325 Pa (real gas). $C_{O_2}^*$ was computed as a function of salinity and temperature according to Garcia and Gordon (1992) using the solubility coefficients derived from the data of Benson and Krause (1984) and converted to values of µmol L^{-1} using a density of 1 kg L^{-1}. Molar concentrations were used because they are independent of temperature and pressure, and facilitate mass balance calculations and modelling.

Chemical analysis

Water samples for dissolved nutrient analysis were filtered directly from the syringes through 0.45 µm cellulose-acetate disc filters (FP30/0.45CA, Whatman) into polyethylene-bottles, immediately placed at 4 °C in darkness and analyzed within 32 h. NO$_3^-$, NO$_2^-$ and NH$_4^+$ were colorimetrically analyzed following standard methods (DEV 2004). NO$_3^-$ was measured after reduction to NO$_2^-$ on a cadmium column with a flow injection analyzer (detection limit: 700 nmol L^{-1}, Skalar SAN+ system, Skalar Analytical) using sulfanilamide and N-(1-naphtyl)-ethylenediammonium chloride. NO$_2^-$ (detection limit: 35 nmol L^{-1}) and NH$_4^+$ (detection limit: 500 nmol L^{-1}) were determined by photometric analysis (Hitachi U-2000 spectrophotometer, Hitachi High Technologies) with a 10 cm cuvette at 543 and 690 nm, respectively.

To analyze dissolved and particulate Mn and Fe, 8 ml of filtered (FP30/0.45CA, Whatman, 0.45 µm pore size) and 8 ml of unfiltered water-sample were collected in Falcon tubes (BD Falcon, BD Biosciences) and acidified with 150 µL of concentrated HNO$_3$ (Suprapur 65 %, Merck). After separate analysis by inductively coupled plasma optical emission spectroscopy (Spectro Arcos ICP-OES, Spectro Analytical Instruments, detection limits: Mn: 2 nmol (257.611 nm), Fe: 4 nmol (238.204 nm)), the particulate Mn and Fe concentrations were calculated by subtracting the dissolved metal-concentrations obtained from the filtered sample from the total metal concentrations obtained from the unfiltered sample.

For analysis of sulphide as ΣH$_2$S (H$_2$S, HS$^-$, S^{2-}) after precipitation as ZnS according to Cline (1969), 2 ml of water-sample was conserved in 1 mL of 4 % Zn acetate in 2 % acetic acid and stored dark at 4 °C until photometric measurement within 32 h with a 1 cm cuvette at 670 nm (detection limit: 2 µmol L^{-1}, Hitachi U-2000 spectrophotometer, Hitachi High Technologies).

Samples for combined measurement of CH$_4$ and N$_2$O were collected in N$_2$-purged and pressurized 60 ml glass-bottles preloaded with ~ 0.1 g copper(I) chloride and closed with new butyl-rubber septa. After on-site pressure equilibration, the sample-volume equivalent of N$_2$ was removed and substituted by up to 35 ml of unfiltered water sample. Dissolved CH$_4$ and N$_2$O were measured on a gas chromatograph (6890N, Agilent Technologies) with a flame ionization detector and an electron capture detector, respectively. Dissolved gas concentrations were calculated using solubility data from Wiesenburg and Guinasso (1979) for CH$_4$ and from Weiss and Price (1980) for N$_2$O.

Lake Rot campaign

On 14 September 2010, samples for reactive nitrogen (NO$_3^-$, NO$_2^-$, NH$_4^+$) and trace gases (CH$_4$, N$_2$O) were retrieved during two consecutive sets of casts that provided up to 12 individual samples. For each set, one low-resolution cast across the whole water column and two high-resolution sampling casts covering the low-oxic to anoxic

transition were performed. Concentrations of dissolved and particulate Mn, Fe and for ΣH_2S were analyzed for all casts. Data are missing for the third syringe in Fig. 4a due to a failed release.

Lake Zug campaign

On 21 July 2010, a synoptic concentration profile spanning the 130−180 m depth-interval was sampled at a low resolution of 1−2 m and concentrations of nutrients, Mn, Fe, N_2O and CH_4 were analyzed. High-resolution sampling-casts across the oxic/anoxic interface providing up to 12 individual water samples were separately performed for nutrient analysis on 25 August 2010 and gas-analysis on 6 August 2010, while Mn, Fe and ΣH_2S-concentrations were analyzed for each cast.

Results

Lake Rot: physical structure and O_2 profiles

The density structure of Lake Rot is governed by strong temperature gradients (Fig. 1a) separating a well-mixed epilimnion with a depth of 4.6 m (Fig. 2b) from a strongly stratified water column below with an average density gradient of 0.4 kg m^{-4} between 5.5 and 8.5 m (Fig. 2b). Depth-deviations between identical density-values were typically less than 40 cm among individual dives.

Epilimnetic O_2 concentrations increased during daytime with a maximum O_2-increase occurring at 2 m depth (Fig. 2a). Between 4.8 and ∼6 m, all profiles show a well-developed and highly reproducible oxycline. The O_2 concentration decreased nearly linearly from 350 to 5 μmol L^{-1} with an average gradient of ∼210 μmol L^{-1} m^{-1} (Fig. 2a). At the lower end of the steep oxycline, however, we observed a 1.5 m thick layer with highly variable low O_2 conditions (Fig. 2c). O_2 peaks of up to 6 μmol O_2 L^{-1} were separated by water with only nanomolar O_2 concentrations. Although vertical O_2-distribution thus varied strongly and sampling locations were changed between individual casts, most peaks appeared at similar relative depths below the oxycline (Fig. 2c). Their alignment further improved when plotted against density (Fig. 2d). As observed in the epilimnion, O_2-concentrations in this low O_2 zone increased with the duration of daylight. Since O_2 dropped below the detection limit several times within the low O_2 zone (Fig. 2c), we operationally defined the oxic/anoxic interface as the deepest location with detected O_2 concentrations above 100 nmol L^{-1}. These positions are located about 1−1.5 m below the lower end of the continuous oxycline in Fig. 2c and are marked in Figs. 1a and 4 with dashed lines. Further details of the casts are summarized in online resource 2.

Lake Rot: gradients of NO_3^-, NO_2^-, N_2O and NH_4^+

Oxidized and reduced N-species co-occurred at the lower end of the steep oxycline at ∼6 m (Fig. 3b, e). Maximum NO_3^- concentrations of up to 20 μmol L^{-1} were measured closely above at 5.5 m (Fig. 4b), but NO_3^- dropped sharply within 40 cm below the oxycline to background concentrations <0.7 μmol L^{-1}. Epilimnetic NO_3^- concentrations were low at 5−7 μmol L^{-1} (Fig. 4a).

Directly below the oxycline in the depth range of decreasing NO_3^- concentrations, narrow NO_2^- and N_2O peaks with maxima of 5 and 150 nmol L^{-1}, respectively, were detected (Fig. 3b, e). NO_2^- vanished together with NO_3^- at 6.4 m (Fig. 4b), while N_2O reached background concentrations at 6.7 m (Fig. 4e).

The gradient of NH_4^+ implies a flux of NH_4^+ from the sediment into the low O_2 zone (Fig. 4a). The NH_4^+ gradient was almost linear above 10 m, it crossed the low O_2 zone apparently unchanged and extended well into the oxic water column (Fig. 3b). In epilimnetic waters, only background concentrations around 0.6 μmol L^{-1} were measured, but due to the missing sample at 4 m (Fig. 4a), the progression of the NH_4^+ gradient as well as the NO_3^- concentrations are underdetermined between 5.5 and 3 m. However, the linear extrapolation of the NH_4^+ gradient of the high-resolution profile (Fig. 3b) reaches background concentrations at ∼5 m and at O_2 concentrations >100 μmol L^{-1}, and the NO_3^- profiles indicate a NO_3^- peak at or above 5.5 m (Figs. 3b, 4a).

Lake Rot: redox gradients of dissolved Mn, Fe, CH_4 and ΣH_2S

The gradients of dissolved Mn and Fe imply a flux from below towards the low O_2 zone (Fig. 4c). Directly at the lower end of the low O_2 zone, the Mn^{2+}-gradient ends and a pronounced particulate Mn-peak is observed. Thus, the Mn (Fig. 3c, f) and less so the Fe profiles (Fig. 3f) show a sharp transition between the reduced and oxidized form at the oxic/anoxic interface located up to 1.5 m below the steep oxycline and show a clear separation from the redox-transition of the N-species (Fig. 3b, e).

The gradient of CH_4 with deep-water concentrations of 800 μmol CH_4 L^{-1} implies a flux of CH_4 from the sediment towards the low O_2 zone (Fig. 4b). CH_4 vanished at the oxic/anoxic interface and thus about 1.5 m below the steep oxycline together with Mn^{2+}, indicating oxidation with O_2 (Fig. 3e, f). As samples were analyzed in parallel for their CH_4- and N_2O-concentrations, the profiles in Figs. 3e and 4b corroborate a clear separation of the zones of CH_4-oxidation and N-cycling. ΣH_2S was detected only below 8.5 m and thus about 1 m below the low O_2 zone (Figs. 3e, 4b, online resource 1).
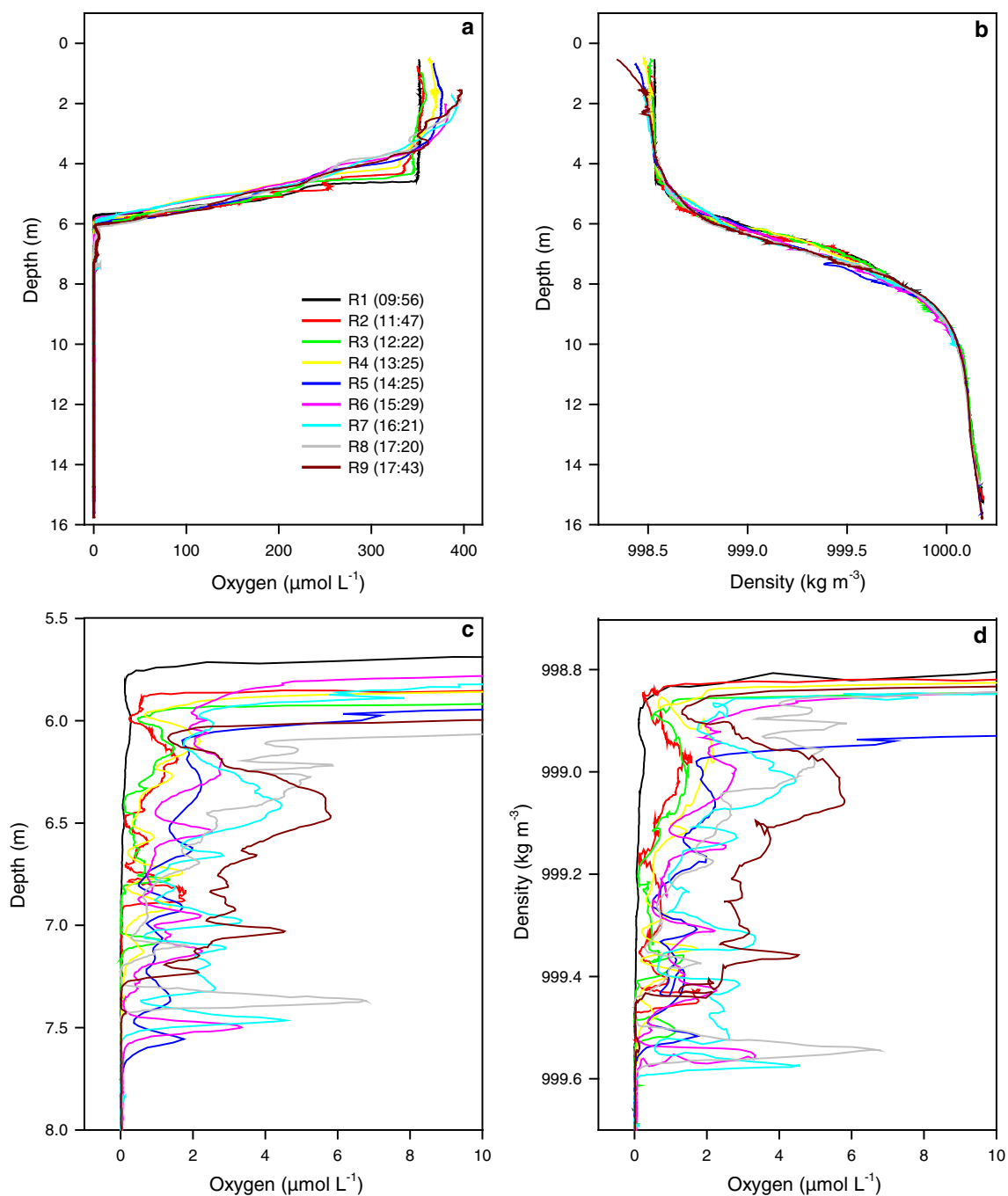
Fig. 2 Lake Rot, 14 September 2010: high-resolution O_2 and density profiles of the water column (**a**, **b**). O_2 profiles enlarged around the lower end of the oxycline (**c**) and density plotted against low O_2 values (**d**). Legend states time of crossing of the oxic/anoxic interface during casts R1−R9

Lake Zug: physical structure and O_2 profiles

In meromictic Lake Zug, the oxic/anoxic transition was located at 150−160 m depth (Fig. 1b). The O_2 concentration decreased nearly linearly for over 100 m towards the oxic/anoxic interface with an average O_2 gradient of

−2.2 μmol L^{-1} m^{-1} (Fig. 1b). Lake Zug's whole hypolimnion was weakly stratified and the position of the oxic/anoxic interface was not associated to any prominent physical feature. The lower end of the weak O_2 gradient in Lake Zug showed a broad submicromolar zone (Fig. 5a, d, g) defined as the water layer in which O_2 concentrations range from 1 to
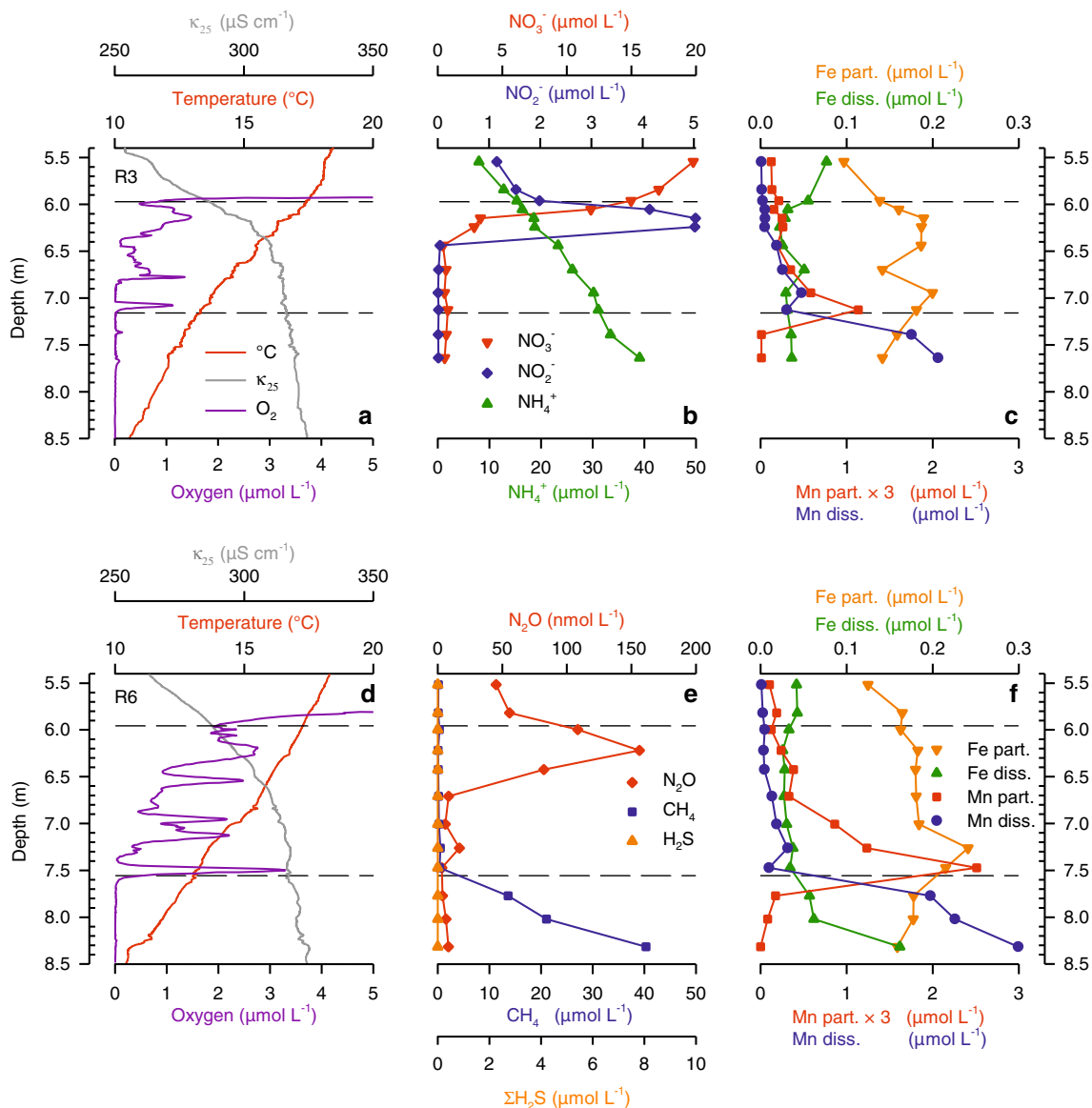
Fig. 3 Lake Rot, 14 September 2010: depth-profiles of cast R3 (*top*) and R6 (*bottom*) across the oxic/anoxic interface showing the distribution of O_2 (**a**, **d**), N-species (**b**, **e**), H_2S and CH_4 (**e**) and transition-metals (**c**, **f**, particular Mn values have been multiplied by 3) together with physical gradients (**a**, **d**). *Dashed lines* indicate the upper and lower boundaries of the low O_2 zone observed directly below the steep oxycline. Redox-horizons of N-species (**b**, **e**), CH_4 (**e**) and transition-metals (**c**, **f**) are closely associated to these boundaries

0.01 µmol O_2 L^{-1}, where the lowest concentration is set by the detection limit of the microoptode. The depth of the oxic/anoxic interface was variable between casts, ranging from 149 to 161 m depth (further details of the casts are summarized in online resource 2). However, the interface was not associated to a specific density layer (data not shown).

The thickness and structure of the submicromolar zone varied in consecutive casts (Fig. 5a, d, g). In cast Z1 (Fig. 5a), O_2 decreased smoothly towards the oxic/anoxic interface at 151 m, but small oxic pockets were detected at 1 and 6 m below the interface. Cast Z10 (Fig. 5d) revealed a ~3 m thick layer with nearly constant nanomolar O_2-levels

situated above a prominent oxic pocket close to the oxic/anoxic interface located at ~156 m. In cast Z11 (Fig. 5g), the position of the oxic/anoxic interface was similar to the previous cast but the thickness of the submicromolar zone was reduced to 1 m. Consecutive O_2 profiles obtained 19 days earlier (Fig. 6a, d, online resource 2) show similar variability in the position, thickness and structure of the submicromolar zone. In summary, the thickness of the submicromolar zones were between 1.7 ± 0.8 m ($n = 9$) and 2.0 ± 0.9 m ($n = 13$) on 6 and 25 August 2010, respectively. Above 1 µmol O_2 L^{-1}, all casts showed steps and small inversions in the O_2 gradients at different depths.
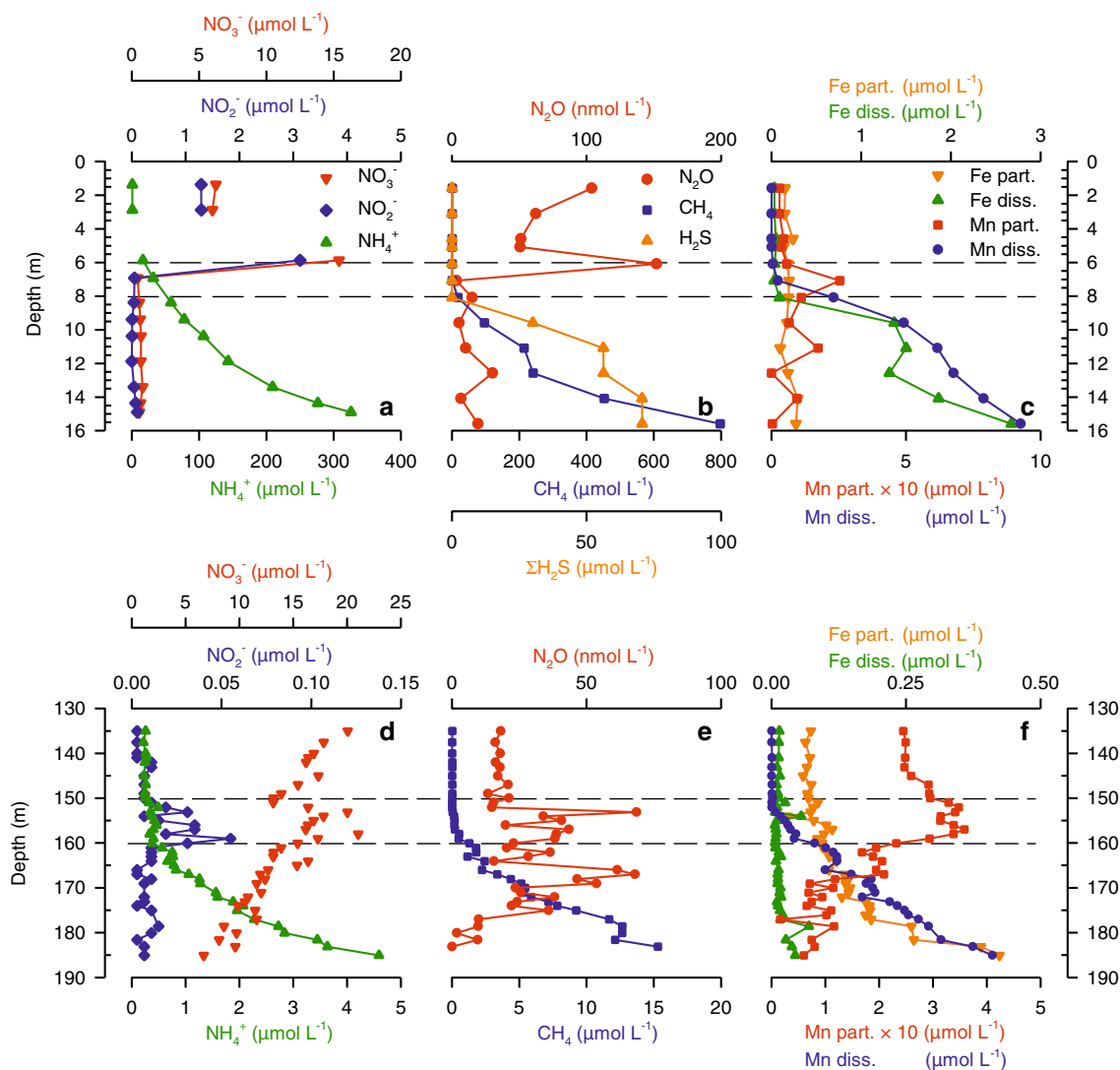
Fig. 4 Synoptical profiles of Lake Rot (*top*) and Lake Zug (*bottom*) showing the distribution of N-species (**a**, **b**, **d**, **e**), CH$_4$ (**b**, **e**), H$_2$S (**b**) and transition-metals (**c**, **f**, particular Mn-values have been multiplied by 10). *Dashed lines* indicate zones with low to submicromolar O$_2$ concentrations. Data is missing for the third syringe in panel **a** due to a failed release

Lake Zug: gradients of NO$_3^-$, NO$_2^-$, N$_2$O and NH$_4^+$

Redox-transformations of NO$_3^-$, NO$_2^-$, and NH$_4^+$ were observed close to the position of the oxic/anoxic interface (Fig. 5b, e, f). But in contrast to Lake Rot, NO$_3^-$ showed no prominent changes across the submicromolar zones but extended to below 180 m (Figs. 5b, e, h, 4d). However, local NO$_3^-$ minima and maxima (Fig. 5e, h) are found at the oxic/anoxic transition where they correspond with 2–4 m broad and concise NO$_2^-$ peaks reaching their maxima of up to 65 nmol L^{-1} either below (Fig. 5e) or at the lower end (Fig. 5b, h) of the submicromolar zone. NH$_4^+$ profiles indicated upward transport of NH$_4^+$ and the resolved end of the NH$_4^+$ gradient was almost linear (Fig. 5b, h). However, NH$_4^+$ concentrations fell below the detection limit at 2–4 m below the oxic/anoxic interface. N$_2$O-concentrations increased close to and below the oxic/anoxic interface (Figs. 6b, e, 4e). But compared to Lake Rot, absolute N$_2$O-concentrations were lower and no distinct peaks were measured.

Lake Zug: redox gradients of dissolved Mn, Fe, CH$_4$ and ΣH$_2$S

The nearly linear gradients of dissolved Mn^{2+} terminated close to the oxic/anoxic interface (Fig. 4f). High resolution profiles show that dissolved Mn is removed already at the lower boundary of the submicromolar zone, indicating effective oxidation at O$_2$ concentrations of less than 200 nmol O$_2$ L^{-1} (Fig. 5c, f, i). Particulate Mn
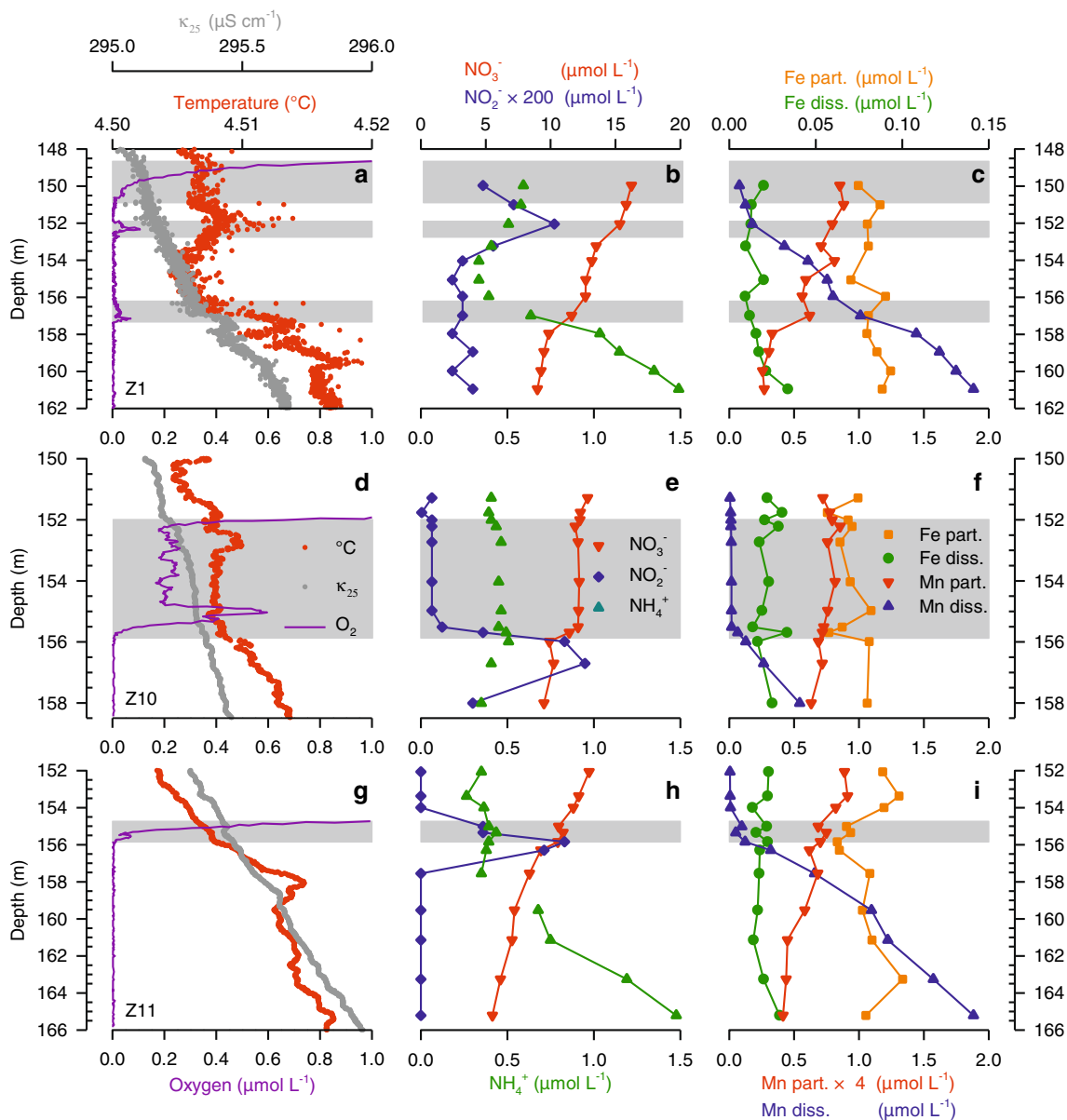
Fig. 5 Lake Zug, 25 August 2010: depth-profiles of casts Z1 (*top*), Z10 (*middle*), and Z11 (*bottom*) across the oxic/anoxic interface showing the distribution of O_2 (**a, d, g**), N-species (**b, e, h**) and transition-metals (**c, f, i**, particular Mn values have been multiplied by 4) together with physical gradients (**a, d, g**). Depths with submicromolar O_2 concentrations are *shaded grey*. Redox-horizons of NO_2^- (**b, e, h**) and dissolved Mn (**c, f, i**) are closely associated to the oxic/anoxic transition, while NH_4^+-concentrations fall below the detection limit (*disconnected triangles*) slightly below the oxic/anoxic transition (**b, h**)

concentrations were elevated in the synoptic profile (Fig. 4f) in a broad zone ($\sim$15 m) around the oxic/anoxic transition at 150−160 m with concentrations falling below 100 nmol L^{-1} at 170 and 100 m depth, respectively. The high-resolution profiles (Fig. 5c, f, i) reveal the lower part of the broad peak of particulate Mn. However, within this large scale gradient local accumulation of particulate Mn could not be observed directly above the interface nor was particulate Mn significantly reduced with the onset of anoxic conditions. Particulate Fe increased below the oxic/

anoxic transition with depth (Fig. 4f), whereas the generally low dissolved Fe concentrations ($\sim$0.025 μmol L^{-1}) increased slightly only below 180 m but showed no clear signs of coupling to the low O_2 zone.

CH$_4$ gradients in Lake Zug were less pronounced than in Lake Rot due to lower absolute concentrations. Similar to Lake Rot, methane was oxidized within the same depth layer as dissolved Mn^{2+}; i.e. in the submicromolar zone and at similar concentrations of around 200 nmol O_2 L^{-1} (Fig. 6e, f). No ΣH_2S was detected in the sampled anoxic water column.
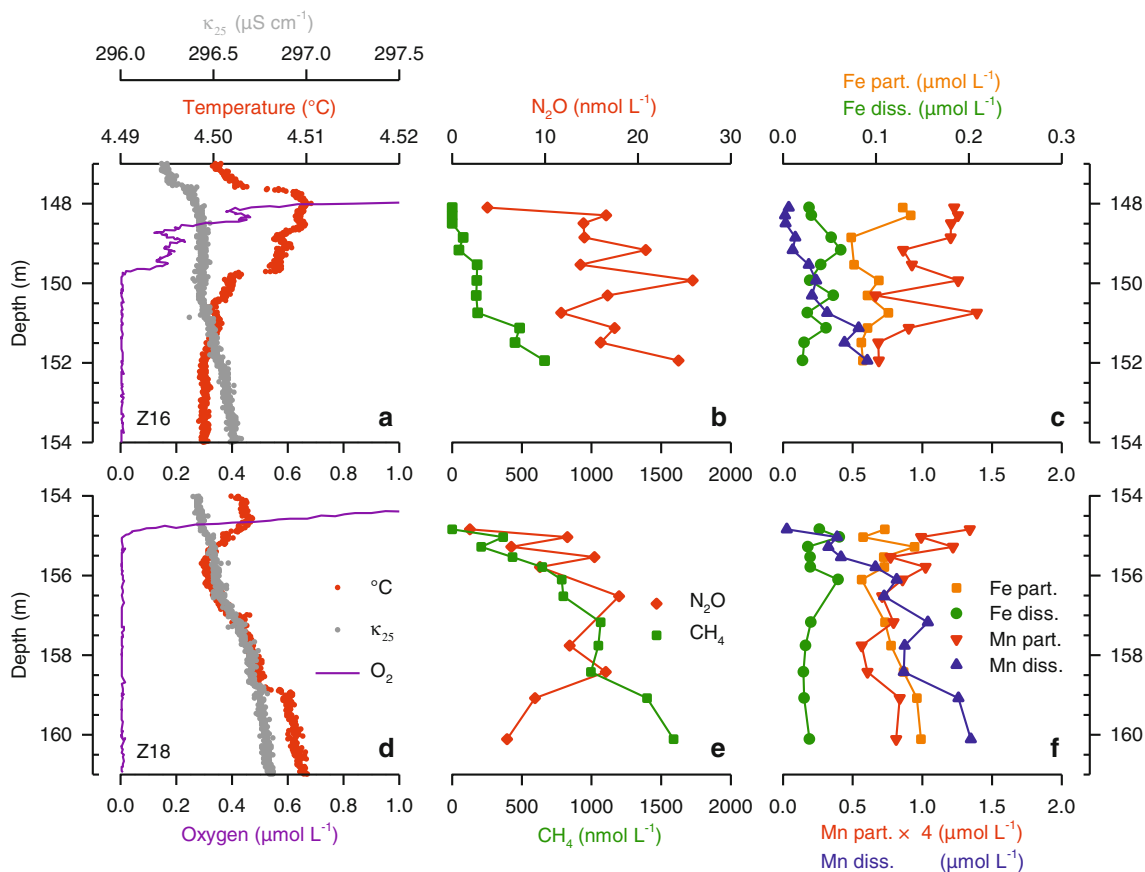
Fig. 6 Lake Zug, 25 August 2010: depth profiles of cast Z16 (*top*) and Z18 (*bottom*) across the oxic/anoxic interface showing the distribution of O_2 (**a, d**), dissolved gases N_2O and CH_4 (**b, e**) and transition-metals (**c, f**, particular Mn-values have been multiplied by 4) together with physical gradients (**a, d**). Depths with submicromolar O_2 concentrations are *shaded grey*. Upward-transported CH_4 (**b, e**) and diss. Mn (**c, f**) are oxidized at submicromolar O_2 concentrations

Discussion

Resolving the submicromolar zone of the oxycline

In seasonally stratified Lake Rot, a low O_2 zone with an extension of about 1 m and distinct O_2-maxima (Figs. 2c, 3a, b) was observed below the steep oxycline (Fig. 2a). The permanently stratified Lake Zug had a weaker synoptic O_2 gradient where extensive zones of submicromolar O_2 concentrations (up to several meters) were visible above the oxic/anoxic interface (Figs. 5a, d, g, 6a, b). The submicromolar zones could not have been resolved with traditional CTD-profiles using electrochemical or optical macro sensors. The existence of extended submicromolar layers imply a significant downward shift of the oxic/anoxic interface compared to estimates deduced from traditional CTD-profiles (Kirf et al. 2013). Without resolving submicromolar concentrations, the linear extrapolation of the O_2-gradient from above 1 to 2 μmol O_2 L^{-1} (the lower detection limit of many sensors) to zero O_2 severely underestimates the true extension of the submicromolar

zone by up to several meters (online resource 2) and lowers the estimated depth of the oxic/anoxic interface. These observations are relevant for the interpretation of suboxic zones that are defined by the absence of both O_2 and H_2S. If revisited with sensitive profiling equipment, such zones will probably turn out to be much thinner or even non-existing and processes like the oxidation of methane might actually occur at submicromolar O_2 concentrations rather than by anaerobic pathways (Canfield and Thamdrup 2009; Bethke et al. 2011; Lehner et al. 2014).

Contributions to the submicromolar O_2 zone

In Lake Zug, profiles were taken in the interior of the deep hypolimnion. Here, turbulence is extremely weak as the energy transfer from large-scale seiching to turbulent mixing occurs in the bottom boundary layer (Goudsmit et al. 1997; Wüest and Lorke 2003). The observed inhomogeneous O_2 distribution, characterized by local maxima and minima in the submicromolar zone, is most likely the

result of lateral transport of water masses with differing source oxygen concentration. Lateral transport is typically 4−5 orders of magnitude more effective than vertical mixing in deep lakes (Peeters et al. 1996). Intermittent reaction, mixing and transport processes can mix up differing water masses in the bottom boundary layer (Lorke et al. 2003; Brand et al. 2008; Müller et al. 2012) and influence the biogeochemical profiles in the interior of a lake by promoting lateral injection of oxygen as known, e.g., from the Black Sea (Konovalov et al. 2003). Lateral transport of water masses with different origin was also indicated by similar variations of temperature and O_2 concentration in some of the profiles (Figs. 5a, 6a).

Variable kinetics of O_2 consuming processes such as microbial respiration, the oxidation of settling organic particles (Wright et al. 2012) and of upward transported reduced chemicals might further shape the submicromolar zone (Thamdrup et al. 2012). As O_2 concentrations decrease with depth, the rates of the various O_2 consuming processes should be increasingly affected according to their different apparent half saturation constants (Stolper et al. 2010; Wright et al. 2012). Consequently, the bulk consumption rate should decrease, which in turn should result in the decrease of O_2 flux and extend the transition zone between the oxic and anoxic water masses: such an extended submicromolar zone should be characterized by a continuous decrease of the O_2 gradient (Fig. 5a, Lake Zug).

Finally, some profiles suggest rather transient O_2 conditions where O_2 intrusions or the oxic/anoxic interface did not yet inflict significant redox-changes. For example, the Mn_2^+ gradient crosses small oxic pockets in cast Z1 (Fig. 5 a, c), while in cast Z16 (Fig. 6b, c), the CH_4 and Mn_2^+ gradient both extend in parallel well across the oxic/anoxic interface. Studies conducted in various aquatic environments with low oxic to anoxic conditions showed that intermittent (lateral) O_2-intrusions can contribute significantly to overall redox-budgets (Zopfi et al. 2001; Konovalov et al. 2003; Schippers et al. 2005) and thus might further sustain aerobic redox-pathways in otherwise anoxic water bodies (Lam et al. 2007; Thamdrup et al. 2012).

In stratified Lake Rot, Secchi-depths of 2.2 and 2.6 m recorded on 16 September 2010 and 9 September 2011 indicate a euphotic depth of 7.4 and 8.1 m, respectively (Tilzer 1988). Sunny weather during the field campaign suggest that the increase of O_2 measured over the day in the epilimnion, the oxycline and the low O_2 zone (Fig. 2a, c) are caused by oxygenic photosynthesis. Patchiness in algal and microbial activity, e.g. originating from intermittent lateral intrusions of water parcels containing microorganisms and O_2 from the bottom boundary layer, could modulate the balance of O_2 production and respiration below the oxycline, eventually explaining the observed

layering of O_2 peaks at specific depths and their stability throughout the day (Fig. 2c). Highly dynamic lateral currents at a stratified pelagic oxycline, despite the lack of turbulent vertical mixing, could be demonstrated recently by Kreling et al. (2014) in a study investigating the vertical O_2 transport across oxyclines and the related fine scale transport processes using a pelagic installation of the eddy correlation technique (Berg et al. 2003). The zone void of detectable O_2 and H_2S found directly below the oxic/anoxic interface (Fig. 3e) might be caused by H_2S-consuming photosynthetic sulphur bacteria that are characteristic for Lake Rot (Kohler et al. 1984).

The O_2 accumulation below Lake Rots oxycline over the day (~ 0.7 mmol m^{-2} h^{-1} estimated from a 4 µmol L^{-1} difference in a 1.5 m thick layer over 8 h, Fig. 2c) is comparable to the flux of O_2 along the oxycline (~ 0.7 mmol m^{-2} h^{-1} for a gradient of 200 mmol m^{-4} and assuming a diffusivity of 10^{-6} m^2 s^{-1} (Schubert et al. 2010)). This additional oxidation-potential below the oxycline should therefore be included in redox-balances on the system-level. Moreover, the calculated O_2 accumulation within the low O_2 zone represents only the net production, whereas the gross O_2-turnover could be substantially higher due to the co-occurrence of O_2 production and consumption.

Redox gradients at the low O_2 boundary

Specific hotspots of redox reactions were related closely to the cast-specific depth of the oxic/anoxic interface (Figs. 3, 5, 6). In both lakes, linear gradients terminating close to the oxic/anoxic interface (CH_4, dissolved Mn^{2+}, Figs. 3, 5, 6) and distinct peaks (NO_2^-, N_2O, particulate Mn in Lake Rot (Fig. 3), NO_2^- in Lake Zug (Fig. 5)) imply that these specific redox horizons have existed over time scales relevant for microbial processes. The position of the chemical gradients and concentration peaks with regards to the O_2 profile indicate that the hitherto unnoticed nanomolar O_2 concentrations do indeed significantly influence redox-cycling. In accordance with recent marine studies (Revsbech et al. 2009; Kalvelage et al. 2011; Thamdrup et al. 2012), this field study confirms that the arbitrarily chosen traditional threshold for the oxic/anoxic transition of 1 µmol O_2 L^{-1} is by at least one order of magnitude too high to adequately detect and classify O_2 dependent redox-interactions in natural systems.

In both lakes, the high-resolution profiles clearly show that O_2 availability in the submicromolar range is a key factor to explain the observed locations of Mn and CH_4 oxidation. Mn^{2+} and CH_4 are consistently oxidized within the same depth-horizon, which is clearly associated to the depth of the oxic/anoxic interface (Figs. 3, 5, 6). Since Mn reacts quickly to changing redox-conditions if microbially

Table 1 Electron-balances of Lake Rot and Lake Zug across the oxic/anoxic transition

Analyte	Lake Rot gradient (mmol m^{-4})	Electron-equivalent gradient (mmol m^{-4})	Lake Zug gradient (mmol m^{-4})	Electron-equivalent gradient (mmol m^{-4})
O_2	−212.0	−848.0	−2.2	−8.8
NO_3^-	−37.2	−186.0	0.21	[a]
NH_4^+	14.2	[a]	0.14	1.12
Dissolved Mn^{2+}	3.3	6.6	0.13	0.25
Dissolved Fe	0.3	0.3	–	–
CH_4	46.0	368.0	0.61	4.88
H_2S	19.5	[a]	–	–
Sum reacting oxidants		−1,034		−8.8
Sum reacting reductants		375		6.3
Total		−659		−2.5

[a] No prominent reaction in low oxygen zone or oxidation by photosynthesis

mediated (Tebo et al. 2004; Jones et al. 2011), the termination of the linear dissolved Mn^{2+}-gradients closely above the oxic/anoxic interface in both lakes corroborates an O_2 dependency of in situ Mn-oxidation (Schippers et al. 2005; Clement et al. 2009).

In contrast to the turnover of Mn^{2+} and CH_4 near the oxic/anoxic interface, the sites of nitrogen cycling were positioned close to the oxycline in Lake Rot (Fig. 2b, e). The linear NH_4^+ concentration gradient (Fig. 3b) suggests that the net flux of NH_4^+ from lower depths to the surface is unaffected by the first appearance of O_2, whereas further above at ∼5 m depth, increased consumption either by algae uptake or by nitrification is indicated by the termination of the NH_4^+ gradient (Figs. 3b, 4a). Schubert et al. (2010) documented similar observations, thus NH_4^+-reactivity appears low at the given environmental conditions below the oxycline. Downward net transport of nitrate decreased directly at the lower end of the steep oxycline, suggesting nitrate reduction which is also supported by the pronounced peaks of NO_2^- at 6.25 m and N_2O slightly below (Fig. 3b, e). Intermediate oxidized N-species thus occurred and disappeared within a narrow layer of only 50 cm (NO_2^-) to 80 cm (N_2O) after O_2-availability severely dropped along Lake Rot steep oxycline. The observed spatial sequence of increasingly reduced N-species follows the sequence expected from the increased sensitivity of N-reducing enzymes towards O_2 (Bonin et al. 1989) and different kinetics of the involved intermediate steps of denitrification (Wild et al. 1995).

NH_4^+-oxidation in Lake Zug was associated to the oxic/anoxic interface (Fig. 5b, e, h). The NH_4^+ gradient from below was almost linear. NH_4^+ concentrations fell below the detection level 2−4 m below the oxic/anoxic interface, but the linearly extrapolated NH_4^+ gradient reaches zero NH_4^+ at the depth horizon of the oxic/anoxic interface (Fig. 5b, h). The depth where the last traces of O_2 disappear, and where ammonium apparently also disappears, is associated with small nitrite-peaks (Fig. 5b, h), presumably formed as a by-product of aerobic ammonium oxidation, and with local maxima of nitrate (Fig. 5h). Aerobic nitrification was found active even at O_2 concentrations below 50 nmol L^{-1} (Kalvelage et al. 2011). However, the small nitrite peak found below the submicromolar zone (Fig. 5e) corresponds to a local nitrate minimum and might indicate co-occurring nitrate reduction.

In Lake Zug, O_2 availability around or below the current detection limit of ∼10 nmol L^{-1} appears sufficient to initiate oxidation of CH_4, Mn^{2+} and NH_4^+. As there is no physical interface associated to the oxic/anoxic interface, the vertical diffusivity can be assumed constant across this layer and can be ignored. Thus, we can construct a flux balance based on the synoptic downward gradients of O_2 on one side and on the upward gradients of CH_4, dissolved Mn^{2+} and NH_4^+ on the other side. The flux balance reveals that the fluxes of CH_4, dissolved Mn^{2+} and NH_4^+ together account for ∼70 % of the O_2 flux when normalized to redox equivalents (Stumm and Morgan 1995) (Table 1). A significant part of this turnover seems to occur within the submicromolar O_2 zone which extended on average over 2 m in Lake Zug.

Conclusions

O_2 measurements with high temporal resolution and sensitivity show that O_2 controls the biogeochemical cycling of N, Mn and CH_4 in dynamic layers with submicromolar O_2 concentrations. Specific hotspots of redox-reactions were found to be closely related to the cast-specific depth of the oxic/anoxic interface. In Lake Zug, O_2 availability around or below the in situ detection limit of ∼10 nmol

O_2 L^{-1} appears sufficient to initiate oxidation of CH_4, Mn^{2+} and NH_4^+ at a water depth of ~ 160 m. Below the steep oxycline of Lake Rot, deep oxygenic photosynthesis could well be responsible for the observed low-level oxygen concentrations which can drive a significant part of the chemotrophic oxidation processes at a water depth of $6-7.5$ m. The historically accepted 1 µmol O_2 L^{-1} detection limit as indicator for anoxic conditions is definitely too high to adequately detect and classify O_2-dependent redox-reactions and to analyze the biogeochemical structure of oxic/anoxic boundaries in natural systems. The new evidence for an extended, heterogeneous and dynamic low-oxygen interface invites more investigations with sensitive profiling devices at proper scales in order to further elucidate microbial pathways and their significance for element cycling across the oxic/anoxic transition. Parts of previously described "suboxic" zones with missing O_2 and H_2S might in fact belong to the realm of oxic processes if characterized with submicromolar sensitivity.

References

Benson BB, Krause D (1984) The concentration and isotopic fractionation of oxygen dissolved in fresh-water and seawater in equilibrium with the atmosphere. Limnol Oceanogr 29(3):620–632. doi:10.4319/lo.1984.29.3.0620

Berg P, Røy H, Janssen F, Meyer V, Jørgensen BB, Huettel M, de Beer D (2003) Oxygen uptake by aquatic sediments measured with a novel non-invasive eddy-correlation technique. Mar Ecol Prog Ser 261:75–83. doi:10.3354/Meps261075

Berner RA (1981) A new geochemical classification of sedimentary environments. J Sediment Petrol 51(2):359–365. doi:10.1306/212F7C7F-2B24-11D7-8648000102C1865D

Bethke CM, Sanford RA, Kirk MF, Jin QS, Flynn TM (2011) The thermodynamic ladder in geomicrobiology. Am J Sci 311(3):183–210. doi:10.2475/03.2011.01

Bonin P, Gilewicz M, Bertrand JC (1989) Effects of oxygen on each step of denitrification on Pseudomonas nautica. Can J Microbiol 35(11):1061–1064

Brand A, McGinnis DF, Wehrli B, Wüest A (2008) Intermittent oxygen flux from the interior into the bottom boundary of lakes as observed by eddy correlation. Limnol Oceanogr 53(5):1997–2006. doi:10.4319/lo.2008.53.5.1997

Canfield DE, Thamdrup B (2009) Towards a consistent classification scheme for geochemical environments, or, why we wish the term 'suboxic' would go away. Geobiology 7(4):385–392. doi:10.1111/j.1472-4669.2009.00214.x

Clement BG, Luther GW III, Tebo BM (2009) Rapid, oxygen-dependent microbial Mn(II) oxidation kinetics at sub-micromolar oxygen concentrations in the Black Sea suboxic zone. Geochim Cosmochim Ac 73(7):1878–1889. doi:10.1016/j.gca.2008.12.023

Cline JD (1969) Spectrophotometric determination of hydrogen sulfide in natural waters. Limnol Oceanogr 14:454–458

DEV (2004) Deutsche einheitsverfahren zur wasser-abwasser- und schlammuntersuchung. Wiley, Weinheim

Garcia HE, Gordon LI (1992) Oxygen solubility in seawater—better fitting equations. Limnol Oceanogr 37(6):1307–1312. doi:10.4319/lo.1992.37.6.1307

Goudsmit GH, Peeters F, Gloor M, Wüest A (1997) Boundary versus internal diapycnal mixing in stratified natural waters. J Geophys Res Oceans 102(C13):27903–27914. doi:10.1029/97JC01861

Gray JS, Wu RSS, Or YY (2002) Effects of hypoxia and organic enrichment on the coastal marine environment. Mar Ecol Prog Ser 238:249–279

Jones C, Crowe SA, Sturm A, Leslie KL, MacLean LCW, Katsev S, Henny C, Fowle DA, Canfield DE (2011) Biogeochemistry of manganese in ferruginous Lake Matano. Indonesia Biogeosciences 8(10):2977–2991. doi:10.5194/bg-8-2977-2011

Kalvelage T, Jensen MM, Contreras S, Revsbech NP, Lam P, Gunter M, LaRoche J, Lavik G, Kuypers MMM (2011) Oxygen sensitivity of anammox and coupled N-cycle processes in oxygen minimum zones. Plos One 6(12):e29299. doi:10.1371/journal.pone.0029299

Keeling RF, Kortzinger A, Gruber N (2010) Ocean deoxygenation in a warming world. Annu Rev Mar Sci 2:199–229. doi:10.1146/annurev.marine.010908.163855

Kirf MK, Dinkel C, Schubert C, Wehrli B (2013) Submicromolar oxygen profiles at the oxic–anoxic boundary of temperate lakes. Aquat Geochem 1–19. doi:10.1007/s10498-013-9206-7

Kohler HP, Ahring B, Albella C (1984) Bacteriological studies on the sulfur cycle in the anaerobic part of the hypolimnion and in the surface sediments of Rotsee in Switzerland. FEMS Microbiol Lett 21(3):279–286. doi:10.1111/j.1574-6968.1984.tb00322.x

Konovalov SK, Luther GW, Friederich GE, Nuzzio DB, Tebo BM, Murray JW, Oguz T, Glazer B, Trouwborst RE, Clement B, Murray KJ, Romanov AS (2003) Lateral injection of oxygen with the Bosporus plume—fingers of oxidizing potential in the Black Sea. Limnol Oceanogr 48(6):2369–2376

Kreling J, Bravidor J, McGinnis DF, Koschorreck M, Lorke A (2014) Physical controls of oxygen fluxes at pelagic and benthic oxyclines in a lake. Limnol Oceanogr 59(5):1637–1650. doi:10.4319/lo.2014.59.5.1637

Lam P, Kuypers MMM (2011) Microbial nitrogen cycling processes in oxygen minimum zones. Annu Rev Mar Sci 3:317–345. doi:10.1146/annurev-marine-120709-142814

Lam P, Jensen MM, Lavik G, McGinnis DF, Müller B, Schubert CJ, Amann R, Thamdrup B, Kuypers MMM (2007) Linking crenarchaeal and bacterial nitrification to anammox in the Black Sea. P Natl Acad Sci USA 104(17):7104–7109

Lashof DA, Ahuja DR (1990) Relative contributions of greenhouse gas emissions to global warming. Nature 344(6266):529–531. doi:10.1038/344529a0

Lehner P, Staudinger C, Borisov SM, Klimant I (2014) Ultra-sensitive optical oxygen sensors for characterization of nearly anoxic systems. Nat Commun 5. doi:10.1038/ncomms5460

Lippitsch ME, Pusterhofer J, Leiner MJP, Wolfbeis OS (1988) Fibre-optic oxygen sensor with the fluorescence decay time as the information carrier. Anal Chim Acta 205(1–2):1–6. doi:10.1016/S0003-2670(00)82310-7

Lorke A, Müller B, Maerki M, Wüest A (2003) Breathing sediments: the control of diffusive transport across the sediment-water

interface by periodic boundary-layer turbulence. Limnol Oceanogr 48(6):2077–2085. doi:10.4319/lo.2003.48.6.2077

Maerki M, Müller B, Dinkel C, Wehrli B (2009) Mineralization pathways in lake sediments with different oxygen and organic carbon supply. Limnol Oceanogr 54(2):428–438. doi:10.4319/lo.2009.54.2.0428

Mulder A, van de Graaf AA, Robertson LA, Kuenen JG (1995) Anaerobic ammonium oxidation discovered in a denitrifying fluidized bed reactor. FEMS Microbiol Ecol 16(3):177–184. doi:10.1111/j.1574-6941.1995.tb00281.x

Müller B, Bryant LD, Matzinger A, Wüest A (2012) Hypolimnetic oxygen depletion in eutrophic lakes. Environ Sci Technol 46(18):9964–9971. doi:10.1021/es301422r

Peeters F, Wüest A, Piepke G, Imboden DM (1996) Horizontal mixing in lakes. J Geophys Res Oceans 101(C8):18361–18375. doi:10.1029/96JC01145

Revsbech NP, Larsen LH, Gundersen J, Dalsgaard T, Ulloa O, Thamdrup B (2009) Determination of ultra-low oxygen concentrations in oxygen minimum zones by the STOX sensor. Limnol Oceanogr Methods 7:371–381. doi:10.4319/lom.2009.7.371

Schippers A, Neretin LN, Lavik G, Leipe T, Pollehne F (2005) Manganese(II) oxidation driven by lateral oxygen intrusions in the western Black Sea. Geochim Cosmochim Ac 69(9):2241–2252. doi:10.1016/j.gca.2004.10.016

Schubert CJ, Lucas FS, Durisch-Kaiser E, Stierli R, Diem T, Scheidegger O, Vazquez F, Müller B (2010) Oxidation and emission of methane in a monomictic lake (Rotsee, Switzerland). Aquat Sci 72(4):455–466. doi:10.1007/s00027-010-0148-5

Seitzinger SP, Nixon SW, Pilson MEQ (1984) Denitrification and nitrous-oxide production in a coastal marine ecosystem. Limnol Oceanogr 29(1):73–83

Stolper DA, Revsbech NP, Canfield DE (2010) Aerobic growth at nanomolar oxygen concentrations. P Natl Acad Sci USA 107(44):18755–18760. doi:10.1073/pnas.1013435107

Stumm W, Morgan J (1995) Aquatic chemistry: Chemical equilibria and rates in natural waters, 3rd edn. John Wiley & Sons, New York, USA

Tebo BM, Bargar JR, Clement BG, Dick GJ, Murray KJ, Parker D, Verity R, Webb SM (2004) Biogenic manganese oxides: properties and mechanisms of formation. Annu Rev Earth Pl Sc 32:287–328. doi:10.1146/annurev.earth.32.101802.120213

Thamdrup B, Dalsgaard T, Revsbech NP (2012) Widespread functional anoxia in the oxygen minimum zone of the Eastern South Pacific. Deep Sea Res Part I 65:36–45. doi:10.1016/j.dsr.2012.03.001

Tilzer MM (1988) Secchi disk—chlorophyll relationships in a lake with highly variable phytoplankton biomass. Hydrobiologia 162(2):163–171

Verbruggen F, Heiri O, Reichart GJ, Lotter AF (2010) Chironomid δ^{18}O as a proxy for past lake water δ^{18}O: a lateglacial record from Rotsee (Switzerland). Quaternary Sci Rev 29(17–18):2271–2279. doi:10.1016/j.quascirev.2010.05.030

Weiss RF, Price BA (1980) Nitrous-oxide solubility in water and seawater. Mar Chem 8(4):347–359

Wiesenburg DA, Guinasso NL (1979) Equilibrium solubilities of methane, carbon-monoxide, and hydrogen in water and seawater. J Chem Eng Data 24(4):356–360

Wild D, von Schulthess R, Gujer W (1995) Structured modeling of denitrification intermediates. Water Sci Technol 31(2):45–54. doi:10.1016/0273-1223(95)00179-Q

Winkler LW (1888) Die Bestimmung des im Wasser gelösten Sauerstoffes. Ber Dtsch Chem Ges 21(2):2843–2854. doi:10.1002/cber.188802102122

Wright JJ, Konwar KM, Hallam SJ (2012) Microbial ecology of expanding oxygen minimum zones. Nat Rev Microbiol 10(6):381–394. doi:10.1038/Nrmicro2778

Wüest A, Lorke A (2003) Small-scale hydrodynamics in lakes. Annu Rev Fluid Mech 35:373–412. doi:10.1146/annurev.fluid.35.101101.161220

Zopfi J, Ferdelman TG, Jørgensen BB, Teske A, Thamdrup B (2001) Influence of water column dynamics on sulfide oxidation and other major biogeochemical processes in the chemocline of Mariager Fjord (Denmark). Mar Chem 74(1):29–51